Letters in Applied NanoBioScience
Open-Access Journal (ISSN: 2284-6808)

Article
Volume 13, Issue 2, 2024, 63
https://doi.org/10.33263/LIANBS132.063

Insights into the Antiproliferative Potentials of Some Plants' Phytochemicals-Molecular Docking and Pharmacokinetics Approaches

Oluwatoba Emmanuel Oyeneyin [1,*], Abiodun Vestor Emmanuel [1], Damilare D. Babatunde [2], Ogunyemi O. Oderinlo [3], Bolawa Fredrick Babatunde [1,4], Gbenga David Omiyeniyi [1], Damilola A. Omoboyowa [5]

[1] Theoretical and Computational Chemistry Unit, Department of Chemical Sciences, Adekunle Ajasin University, Akungba-Akoko, Ondo State, Nigeria
[2] Department of Chemistry, University of Ibadan, Oyo State, Nigeria
[3] Department of Chemistry, Federal University, Otuoke, Bayelsa State, Nigeria
[4] Department of Plant Science and Biotechnology, Adekunle Ajasin University, Akungba-Akoko, Ondo state, Nigeria
[5] Department of Biochemistry, Adekunle Ajasin University, Akungba-Akoko, Ondo state, Nigeria
* Correspondence: oluwatoba.oyeneyin@aaua.edu.ng; emmanueltoba90@gmail.com;

Scopus Author ID 57204181612
Received: 7.03.2023; Accepted: 31.03.2023; Published: 30.06.2024

Abstract: Cancer remains one of the leading causes of death worldwide. Breast cancer, in particular, continues to pose a threat to both developed and developing countries. It accounts for 1 in 8 cancer diagnoses and remains the number one cause of death relating to cancer in women globally. Treatment of cancers with plant and plant-derived products are well embraced for their cost effectiveness, reduced adverse effects, and structural diversities. They are thus the ideal source for developing novel treatments that can address some of the associated challenges with conventional chemotherapies. However, as in most cases, the molecular mechanisms underlying the actions of these plant phytochemicals are not delineated. Therefore, this study aims to understand the potential mode of action of various phytochemicals from plants reportedly used to treat breast cancer. These plant secondary metabolites were tested against the epidermal growth factor receptor (EGFR) tyrosine kinase domain using molecular docking and molecular dynamics simulation. The results showed that echinacoside (-13.65 kcal/mol), quercitrin (-11.42 kcal/mol), and a polyphenol, 2-HPHOT (-9.52 kcal/mol), have higher binding energies in the active site of the EGFK tyrosine kinase than erlotinib (-9.20 kcal/mol), a reference anti-cancer drug. Furthermore, the molecular dynamics simulation parameters derived from the protein-ligand complex showed that echinacoside and 2-HPHOT were stable. These findings demonstrated that these compounds can potentially inhibit EGFR tyrosine kinase and could serve as anti-breast cancer agents.

Keywords: cancer; breast cancer; Chinese plants; computational chemistry; epidermal growth factor receptor.

1. Introduction

Cancer has become a global menace threatening human existence and health. About 10 million new cancer cases were recorded in 2020 [1]. Cancer of the breast is an erratic growth and proliferation of cells in the breast tissue. It can be divided into in situ breast cancer and invasive breast cancer (invaded) [2-4]. Breast cancer is the most pervasive cancer in women

and generally the second most prevalent cancer globally. There were approximately 2.3 million cases of breast cancer and about 685,000 deaths in 2020 globally [5,6]. High consumption of alcohol [7], continual use of birth control pills and tobacco [8], and low intake of vegetables and fruits [9] are some of the causes of breast cancer.

Drugs approved by the Food and Drug Administration (FDA) for effective breast cancer treatments include 5-fluorouracil, epirubicin, docetaxel, doxorubicin, carboplatin, tamoxifen, etc. However, these drugs have side effects such as bone and muscular pain, numbness of feet and hands, loss of libido, vertigo, hair loss, sleep disturbance, lack of concentration, and so on [10,11]. These drawbacks necessitated the shift towards medicinal plants and plant-derived products to prevent and treat this disease because of their great therapeutic activities, abundance, and little or no side effects.

Plants are crucial sources of many biologically active molecules and provide unique chemical templates for drug discovery. Researchers have continued to look for more medicinal plants with great therapeutic and biological activities to treat breast cancer. Chinese plants such as *Allium satium,* one of the oldest plants, have been used as food and also serve as herbal medicine for colds, asthma, and respiratory infections owing to some sulfur-containing phytochemicals such as allicin, ajoene, allyl-methyl trisulfide and derivatives and so on present in it [12,13], it has also been reported for its anti-cancer potentials [14]. *Echinacea purpurea* has been reported for its pharmacological activities such as anti-cancer, anti-HIV, antimicrobial, and wound healing; its major constituents are echinacoside, caffeic acid, cichoric acid, caftaric acid, and so on [15]. *Curcuma longa* is another plant containing active ingredients such as curcumin and some phenolic substances responsible for diverse medicinal properties [13], even anti-cancer [14]. Burdock (*Arctium lappa*) is a plant containing arctigenin as its active phytochemical [13] and has also been reported for its anti-cancer potentials [16]. Others include ginger (*Zingiber officinale*), whose major constituent is 6-gingerol [17], and neem (*Azadiracta Indica*), containing Nimbolide as its active component [18,19]. Therefore, this study aimed to investigate the mechanisms of action of some phytochemicals in a myriad of plants reported for anti-cancer activity using molecular docking and Molecular Dynamic (MD) simulation (see a full list of plants and their bioactive components considered in Table 1).

Table 1. Phytochemicals present in the plants above.

Plant	Phytochemical	IUPAC	Structure	References
Allium satium	Allicin (65036)	3-prop-2-enylsulfinylsulfanylprop-1-ene	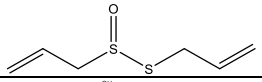	[12,13]
Echinacea purpurea	Echinacoside (5281771)	[(2*R*,3*R*,4*R*,5*R*,6*R*)-6-[2-(3,4-dihydroxyphenyl)ethoxy]-5-hydroxy-2-[[(2*R*,3*R*,4*S*,5*S*,6*R*)-3,4,5-trihydroxy-6-(hydroxymethyl)oxan-2-yl]oxymethyl]-4-[(2*S*,3*R*,4*R*,5*R*,6*S*)-3,4,5-trihydroxy-6-methyloxan-2-yl]oxyoxan-3-yl] (*E*)-3-(3,4-dihydroxyphenyl)prop-2-enoate	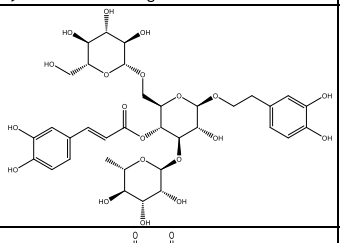	[13]
Curcuma longa	Curcumin (969516)	(1*E*,6*E*)-1,7-bis(4-hydroxy-3-methoxyphenyl)hepta-1,6-diene-3,5-dione	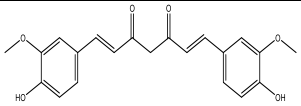	[13]

Arctium lappa	Arctigenin (64981)	(3*R*,4*R*)-4-[(3,4-dimethoxyphenyl)methyl]-3-[(4-hydroxy-3-methoxyphenyl)methyl]oxolan-2-one	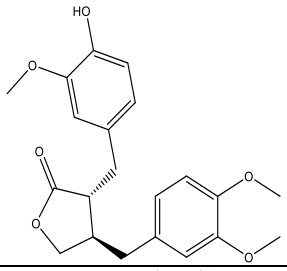	[13]
Zingiber officinale	6-gingerol (3473)	5-hydroxy-1-(4-hydroxy-3-methoxyphenyl)decan-3-one	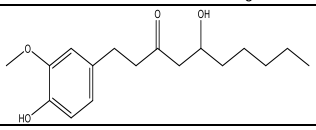	[17]
Azadiracta Indica	Nimbolide (10017)	methyl 2-[(1*R*,2*S*,4*R*,6*R*,9*R*,10*S*,11*R*,15*R*,18*R*)-6-(furan-3-yl)-7,9,11,15-tetramethyl-12,16-dioxo-3,17-dioxapentacyclo[9.6.1.$0^{2,9}$.$0^{4,8}$.$0^{15,18}$]octadeca-7,13-dien-10-yl]acetate	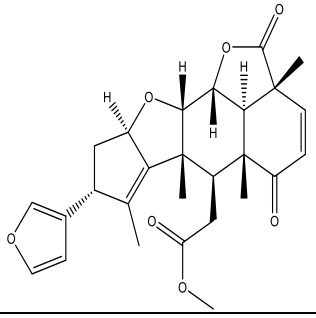	[18,19]
Rhus coriaria	Quercitrin (5280459)	2-(3,4-dihydroxyphenyl)-5,7-dihydroxy-3-[(2*S*,3*R*,4*R*,5*R*,6*S*)-3,4,5-trihydroxy-6-methyloxan-2-yl]oxychromen-4-one	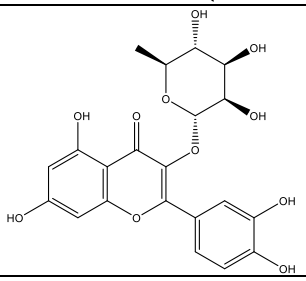	[20]
Cirullus colocynthis	Cucurbitacin I (5281321)	(8*S*,9*R*,10*R*,13*R*,14*S*,16*R*,17*R*)-17-[(*E*,2*R*)-2,6-dihydroxy-6-methyl-3-oxohept-4-en-2-yl]-2,16-dihydroxy-4,4,9,13,14-pentamethyl-8,10,12,15,16,17-hexahydro-7*H*-cyclopenta[a]phenanthrene-3,11-dione	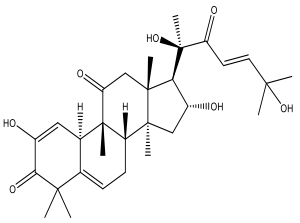	
Myrtus communis	2-HPHOT (5321884)	(2S,3R,4S,5S,6R)-2-[2,4-dihydroxy-6-[(E)-2-(4-hydroxyphenyl)ethenyl]phenoxy]-6-(hydroxymethyl)oxane-3,4,5-triol (2-HPHOT)	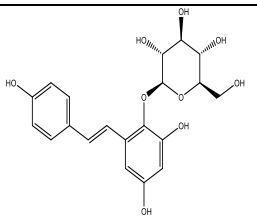	[21]

2. Materials and Methods

2.1. Protein and ligand preparation, docking, and MMGBSA.

The crystal protein structure of an epidermal growth factor receptor (EGFR) tyrosine kinase domain, 1M17 (resolution of 2.6 Å), together with its co-crystallized ligand, erlotinib which is also the reference anti-cancer drug, was retrieved from PDB (www.rcsb.org). The protein was prepared using the protein preparation wizard to remove specific errors by fixing missing hydrogen atoms and assigning bond orders [22]. This is followed by site mapping and a glide grid to generate the actual position of the co-crystallized ligand in the protein, the active site (x = 22.01, y = 0.25, z = 52.79) [23]. The molecules and erlotinib were prepared and docked

at the protein's active site using the extra precision (XP) docking according to the guide provided earlier [24,25]. Erlotinib (figure 1) was re-docked for validation. The Ramachandran plot of the EGFR was plotted (figure 2).

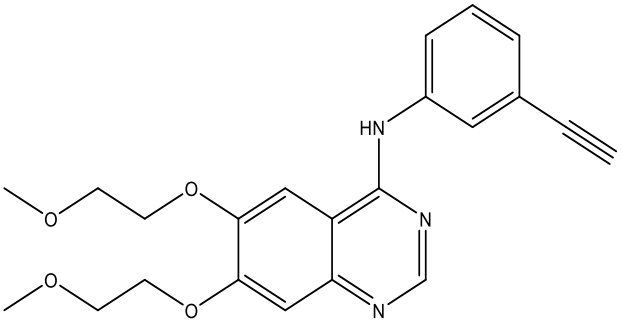

Figure 1. Erlotinib.

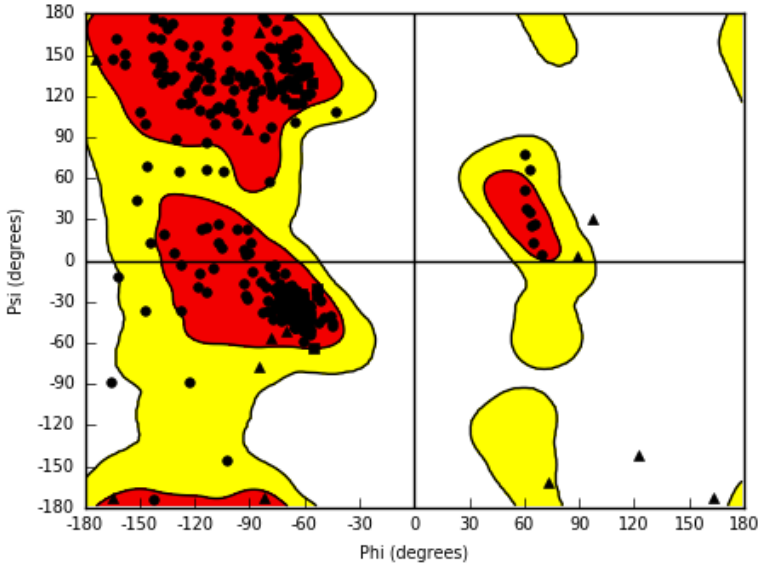

Figure 2. Ramachandran plot of the retrieved crystal protein structure (1M17) from PDB repository.

Minimization of the ligands-1M17 complexes was done using Prime. The binding energy (Δ^{bind}) for all ligands-1M17 complexes was determined using the OPLS3 force field. The molecular mechanics generalized Born surface area (MMGBSA) was obtained from the complexes, while the binding free energy was obtained using Equation 1.

$$.\Delta GBind = \Delta EMM + \Delta GSolv + \Delta GSA \quad (1)$$

2.2. AutoQSAR model.

The experimental dataset containing EGFR tyrosine kinase domain (1M17) inhibitors were retrieved together with their IC_{50} from (www.ebi.ac. uk/chembl/) and converted to .sdf using the Data-Warrior package (v.2) [26]. The .sdf files were minimized on the workspace of the Schrodinger suite. The QSAR model was performed from the pIC_{50} of the compounds. Kpls_molprint2D_26 model was selected because it has the ranking amongst others. Parameters like ranking score, standard deviation, R^2, Q^2, and RMSE were used to assess the model [26].

2.3. MD Simulations.

The complex of the EGFR kinase domain and the molecules with the highest docking scores were subjected to MD simulation to evaluate their binding efficacy, such as conformation and structural changes, to illustrate the effect of the inhibitors binding on the internal dynamics of the kinase domain. The initial coordinates of the receptor include EGFRK and forty amino acids from the carboxyl-terminal tail (PDB accession code 1M17). After placing the inhibitor molecules between the NH_2 and COOH terminal lobes of the receptor, solvation of the models was done using the CHARMM TIP3P water model, with salt ions (Na^+ and Cl^-) introduced at concentrations of 150mM, resulting in electro-neutral systems. The solvated complexes were then subjected to energy minimization using 5000 steps of the steepest descents method to resolve bad contacts and clashes in the system. Convergence of the minimization was ascertained at a potential energy of $1.8593x10^6$ kcal $mol^{-1}Å^{-1}$. Following the energy minimization, the systems were equilibrated for 5ns at 303.15K using NVT ensemble. In the present study, the complexes underwent a production run of 100 ns, saving the coordinates at every 2 fs while evaluating the bonded interactions at every 2 fs at constant temperature (303.15 K) using a Berendsen thermostat [27] with a time coupling constant of 1.0 ps^{-1}. The pressure was controlled at 1.0 bar using a Parrinello-Rahman barostat [28] with velocities and energies saved at every 100ps. The vibrations of all the hydrogen atoms were constrained using the LINCS algorithm [29].

All MD simulations in the present study were performed with GROMACS 2021.5 [30] using CHARMM36 all-atom force field. Topologies and parameter files of the lead compounds, the standard inhibitor and the receptor, were generated using Charmm-gui's solution builder server [31]. MD result analysis: RMSD, RMSF, Radius of Gyration, and Solvent Area were performed using gmx analysis tools.

3. Results and Discussion

3.1. Molecular docking and obtained binding free energy.

Molecular docking is a technique used in drug design and discovery to screen structures. It helps predict potential drug targets and probes into molecule-receptor interactions [32]. It has become a dependable tool for the pharmaceutical industry to identify novel drug candidates before pre-clinical and clinical trials. Erlotinib was docked at the active site of the receptor, 1M17, in a bid to validate the docking procedure. Figure 3 represents the superimposed erlotinib with RMSD as 0.82 Å less than 2.0 Åimplying that the docking procedure is reproducible and reliable [26]. The docking scores and the binding free energies of the compounds and co-crystallized ligands are shown in Figure 4. Echinacoside (-13.65 kcal/mol), quercitrin (-11.42 kcal/mol), 2-HPHOT (-9.52 kcal/mol), have higher binding energies than Erlotinib (-9.20 kcal/mol).

Table 2, and Figure 5 display the interactions between the compounds and the receptor's amino acid residues. Echinacoside formed 9 hydrogen bonds with GLU 739; ASP 831; ASN 818; GLU 790; PRO 770 via its hydroxyl groups, while quercitrin formed 4 hydrogen bond interactions with ARG 818; MET 769; ALA 719; GLU 738, also via its hydroxyl groups. Polyphenol also formed 4 hydrogen bonds (ALA 719; THR 830; LYS 721; ASP 831) via hydroxyl and ether oxygen. Erlotinib formed 2 hydrogen bonds with CYS 773;

GLN 767 via one of its methoxyethoxy oxygens and quinazolin-4-amine nitrogen groups. Echinacoside, quercitrin, and 2-HPHOT are the hits from all the compounds investigated.

The MMGBSA method allows the calculation of the binding free energy of small ligands to biological macromolecules. They have been successful with a lot of molecular systems [33]. The free binding energy values of the complexes of the compounds and receptor (figure 4) reveal that echinacoside (-65.89) has the highest negative value for the MMGBSA followed by erlotinib (-58.70), quercitrin (-48.01), and 2-HPHOT (-38.73). In both docking scores and MMGBSA, echinacoside has higher values than erlotinib.

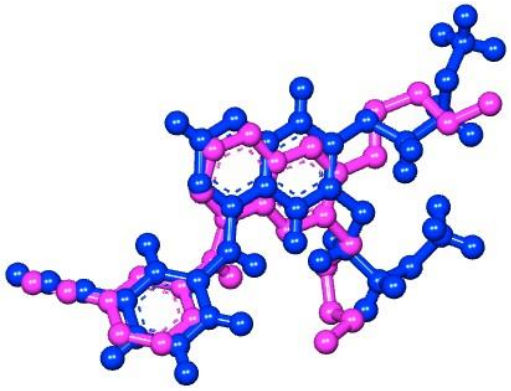

Figure 3. Erlotinib superimposed with its docked pose (RMSD = 0.82 Å).

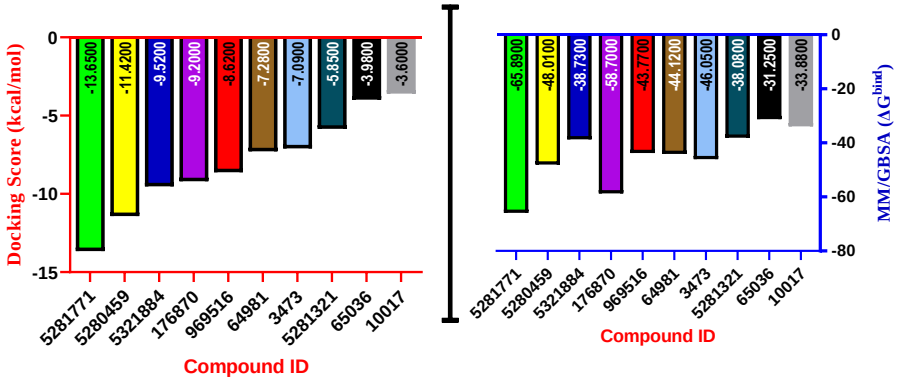

Figure 4. Docking score and Binding energy (ΔG^{bind}) of compounds and erlotinib. 5281771-Echinacoside; 5280459-Quercitrin; 5321884-2-HPHOT; 176870-Erlotinib; 969516-Curcumin; 64981-Arctigenin; 3473-6-gingerol; 5281321-Cucurbitacin I; 65036-Allicin; 10017-Nimbolide.

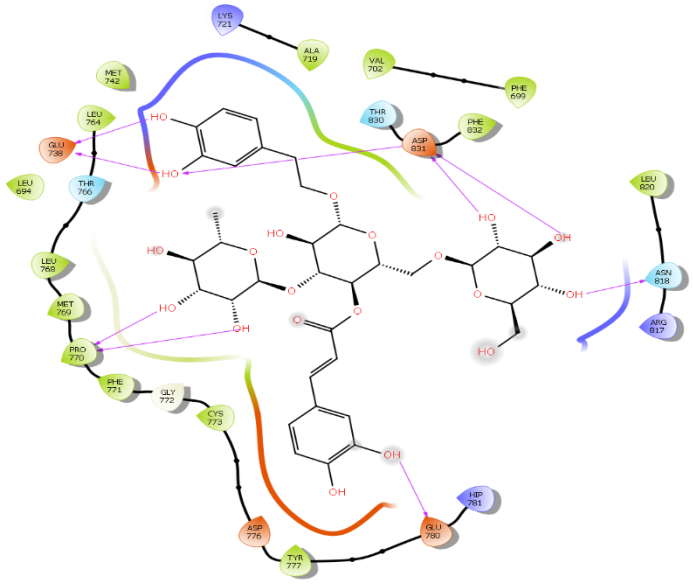

a

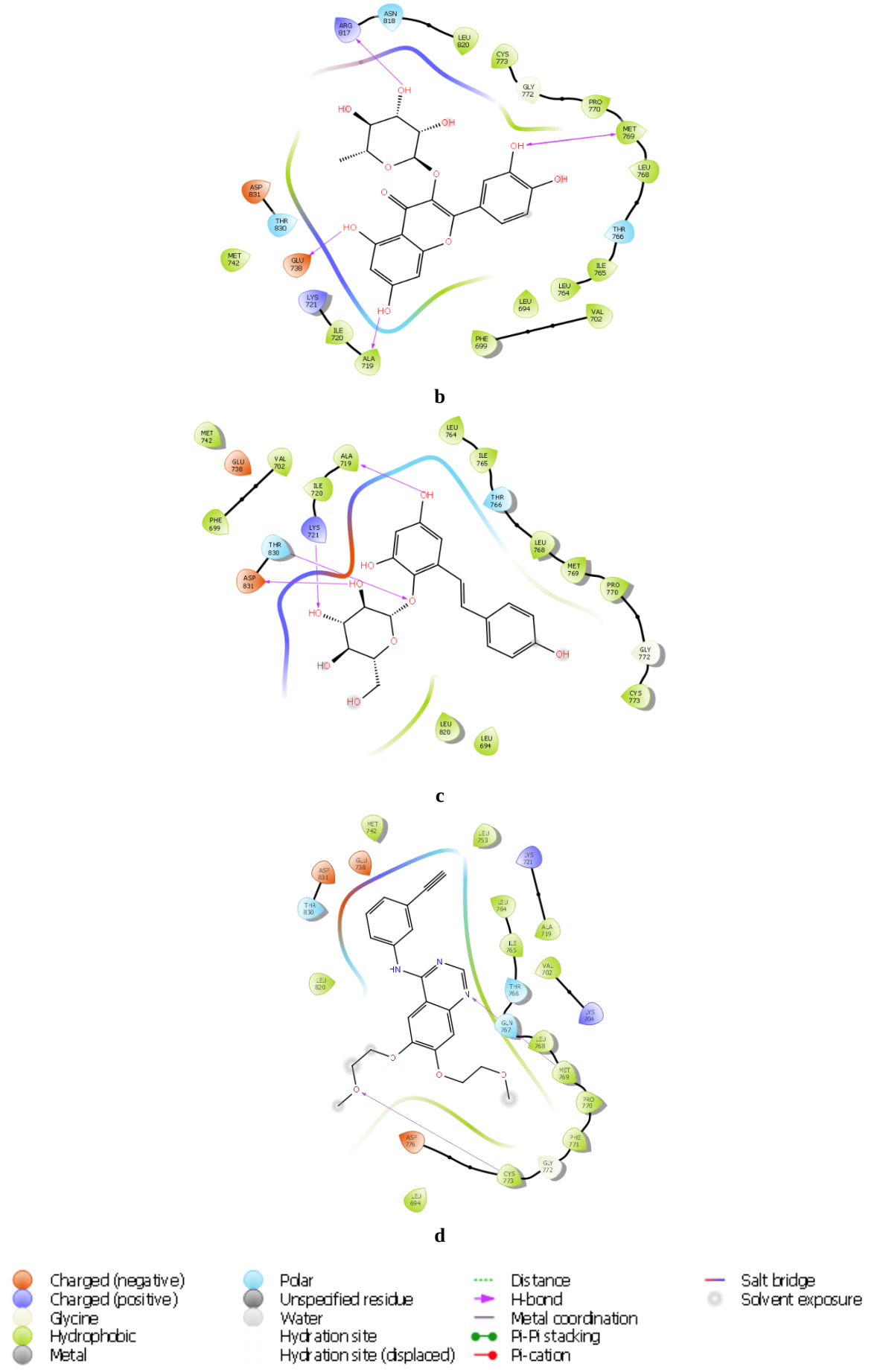

Figure 5. 2D interactions of molecules with high docking scores viz; (a) 5281771-Echinacoside; (b) 5280459-Quercitrin; (c) 5321884-2-HPHOT; (d) 176870-Erlotinib.

Table 2. Hydrogen bond interaction of the docked complex.

Compounds	Number of H-bonds	Residues
Echinacoside	9	GLU 739; ASP 831; ASN 818; GLU 790; PRO 770
Quercitrin	4	ARG 818; MET MET 769; ALA 719; GLU 738
2-HPHOT	4	ALA 719; THR 830; LYS 721; ASP 831
Erlotinib	2	CYS 773; GLN 767
Curcumin	2	MET 769; ASP 776
Arctigenin	2	ASP 831; MET 769
6-gingerol	2	MET 769
Cucurbitacin I	4	ASP 776; MET 769; ASP 831
Allicin	1	MET 769
Nimbolide	1	CYS 773

3.2. AutoQSAR.

QSARs are mathematical equations used to predict the activity/property of compounds by using the descriptors of the compounds [34-36]. AutoQSAR is an algorithm in the Schrodinger suite that uses molecular descriptors to build models [26]. The experimental compounds were divided into 23.6% test and 76.4% train sets (table 4). The model with the best prediction is the kpls_molprint2D_26, with standard deviation (0.5907), R^2 (0.7704), RMSE (0.7485), and Q^2 (0.5481) (table 3). The correlation between the predicted and observed activity is presented as a scattered plot (figure 6). The compounds' pIC_{50} was predicted with the model and presented (table 5). The pIC_{50} of the compounds with the highest docking scores and reference ligand is above 5.00 µM, with the standard ligand (erlotinib) having the highest pIC_{50} (7.04 µM). Among the active compounds from different plants, quercitrin (5.78 µM), cucurbitacin I (5.77 µM), and allicin (5.77 µM) possess the most satisfactory predicted pIC_{50} against the target.

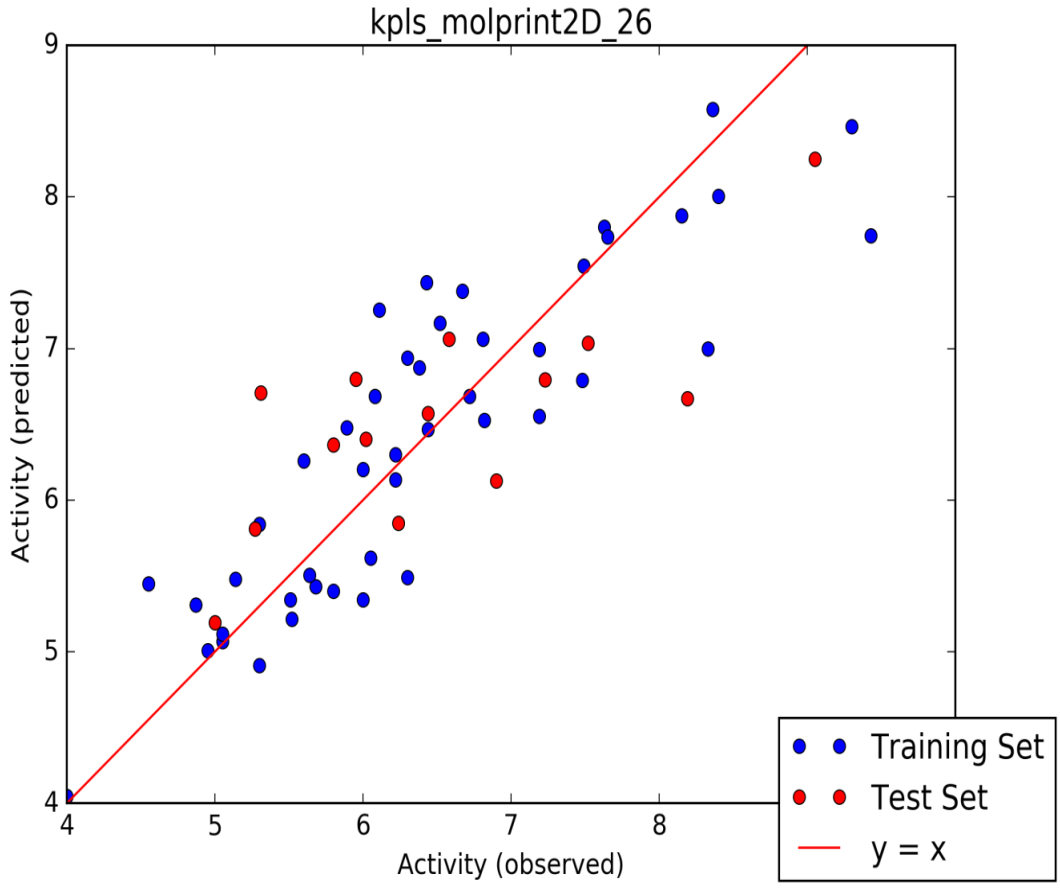

Figure 6. Scatter plot of kpls_molprint2D_26.

Table 3. Parameters of kpls_molprint2D_26.

Model	S.D	R^2	RMSE	Q^2
kpls_molprint2D_26	0.5907	0.7704	0.7485	0.5481

Table 4. Predicted and observed activities from kpls_molprint2D_26.

ID	Set	Observed pIC_{50}	Predicted pIC_{50}	Residual
1	Train	7.1900	6.9956	-0.1944
2	Train	6.0800	6.6839	0.6039
3	Train	7.4900	7.5453	0.0553
4	Train	7.6300	7.8001	0.1701
5	Train	6.3800	6.8761	0.4961
6	Test	6.4400	6.5723	0.1323
7	Train	6.4300	7.4360	1.0060
8	Train	5.6000	6.2606	0.6606
9	Test	5.8000	6.3643	0.5643
10	Train	6.2200	6.3021	0.0821
11	Train	6.4400	6.4656	0.0256
12	Train	5.8900	6.4802	0.5902
13	Train	9.3000	8.4659	-0.8341
14	Train	8.3600	8.5773	0.2173
15	Test	9.0500	8.2510	-0.7990
16	Train	6.6700	7.3800	0.7100
17	Train	6.7200	6.6839	-0.0361
18	Test	6.9000	6.1272	-0.7728
19	Train	8.1500	7.8756	-0.2744
20	Train	8.4000	8.0045	-0.3955
21	Train	4.0000	4.0452	0.0452
22	Train	5.3000	4.9081	-0.3919
23	Train	6.8100	7.0612	0.2512
24	Test	5.9500	6.7985	0.8485
25	Test	5.0000	5.1929	0.1929
26	Test	5.3100	6.7075	1.3975
27	Train	5.8000	5.3991	-0.4009
28	Train	6.0500	5.6200	-0.4300
29	Train	5.6800	5.4313	-0.2487
30	Train	6.2200	6.1354	-0.0846
31	Test	5.2700	5.8094	0.5394
32	Train	4.9500	5.0059	0.0559
33	Test	7.5200	7.0370	-0.4830
34	Train	6.0000	6.2025	0.2025
35	Train	6.3000	5.4912	-0.8088
36	Test	6.5800	7.0640	0.4840
37	Train	9.4300	7.7436	-1.6864
38	Train	8.3300	6.9969	1.3331
39	Train	6.8200	6.5289	-0.2911
40	Train	5.6400	5.5056	-0.1344
41	Train	6.3000	6.9369	0.6369
42	Test	6.2400	5.8492	-0.3908
43	Test	8.1900	6.6697	-1.5203
44	Train	5.5100	5.3451	-0.1649
45	Train	5.5200	5.2159	-0.3041
46	Train	5.0500	5.0679	0.0179
47	Train	5.1400	5.4787	0.3387
48	Train	6.0000	5.3451	-0.6549
49	Train	7.4800	6.7899	-0.6901
50	Train	5.0500	5.1182	0.0682
51	Test	7.2300	6.7935	-0.4365
52	Train	7.1900	6.5554	-0.6346
53	Train	4.5500	5.4481	0.8981
54	Train	5.3000	5.8394	0.5394
55	Train	6.5200	7.1691	0.6491
56	Test	6.0200	6.4043	0.3843
57	Train	4.8700	5.3090	0.4390
58	Train	6.1100	7.2560	1.1460
59	Train	7.6500	7.7375	0.0875

Table 5. Predicted pIC_{50} of the compounds.

Pubchem number	Compound Name	Predicted pIC_{50} (μM)
5281771	Echinacoside	5.51
5280459	Quercitrin	5.78
5321884	Polyphenol	5.37
176870	Erlotinib	7.04
969516	Curcumin	5.68
64981	Arctigenin	5.28
3473	6-gingerol	5.53
5281321	Cucurbitacin I	5.77
65036	Allicin	5.77
10017	Nimbolide	5.32

3.3. Molecular dynamics simulations.

After running for 100 ns, MD simulations of the protein (apo- and ligand-bound forms) showed various dynamic properties of the inhibitors in their bound states (Figure 7). Specifically, the Cα root mean square deviations (RMSDs) of some of the compounds showed low fluctuations and remained stable until the end of the simulation time. $EGFRK_{176870}$ complex had the highest fluctuation, which showed instability of the compound in the system. Followed by $EGFRK_{5280459}$, after variable trajectory, it plateaued at 45 ns to 0.5 Å, then with little fluctuation until 56 ns; it remained stable until the end of the simulation. Meanwhile, $EGFRK_{5321884}$ and $EGFRK_{5281771}$ systems showed lower fluctuation with stable trajectory. Importantly, the mean Cα root mean square fluctuations (RMSFs) of each residue were evaluated in the protein to address the increased flexibility. In this study, we have considered the catalytic residues that should be less flexible within the kinase domain share in the EGFRK binding pocket [37]. Most residues in $EGFRK_{5321884}$ regions showed lower flexibility than others (Figure 8), while the $EGFRK_{176870}$ complex showed the highest deviations. The structural flexibilities of all the EGFRK systems were comparable.

During the simulations, the gyration radius (Rg) of $EGFRK_{5281771}$ and $EGFRK_{5321884}$ complexes was consistent through the simulation, as shown in Figure 9, indicating the stability of the complexes and the also absolves the ligand of causing any significant changes in the folding pattern of the protein. The average Rg values were 2.44 Å, 2.47 Å, 2.19 Å, 2.12 Å, and 2.09 Å for $EGFRK_{APO}$ and its bound complexes of $EGFRK_{176870}$, $EGFRK_{5280459}$, $EGFRK_{5281771}$, and $EGFRK_{5321884}$, respectively, confirming that the compactness of the structures is close.

The stability of the complexes can also be evaluated from the protein's surface (in solvent) conformational changes during energy interaction simulation that can be verified through the complex Solvent Accessible Surface Area (SASA) in Figure 10. The calculated SASA of EGFRK protein was considered through the 100 ns simulation trajectory period to explore the role of the hydrophilic and hydrophobic forces and residues on the solvent. The calculated average SASA value of the complex $EGFRK_{176870}$, $EGFRK_{5280459}$, $EGFRK_{5281771}$, $EGFRK_{5321884}$, and $EGFRK_{APO}$ were 177.14 $Å^2$, 177.46 $Å^2$, 177.94 $Å^2$, 174.65 $Å^2$, and 184.18 $Å^2$ respectively. Reduced SASA values indicate that the protein/ligand has shrunk relative to the solvent surface charges, resulting in more compact and stable conformations. $EGFRK_{5321884}$ shows that the solvent-exposed area is stable.

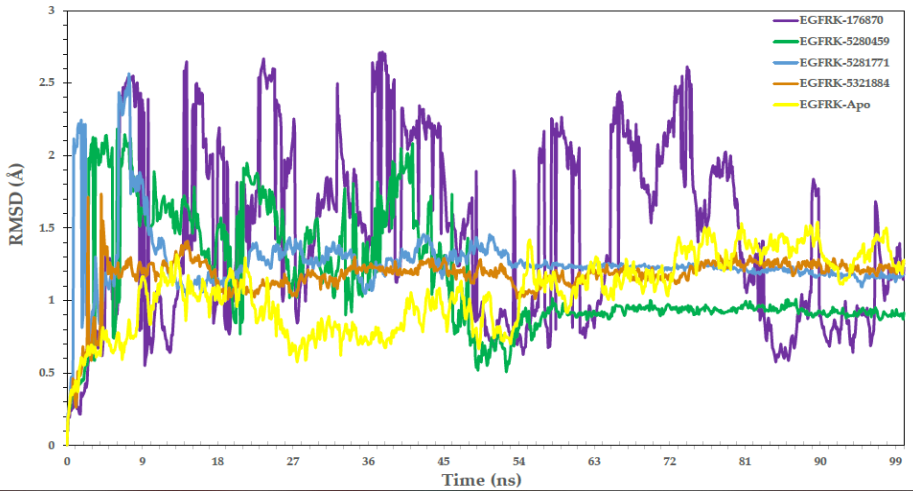

Figure 7. Time-evolution RMSD of the Cα atoms of the four investigated complexes compared to the Protein's Apo structure over 100 ns. Trajectories for $EGFRK_{176870}$, $EGFRK_{5280459}$, $EGFRK_{5281771}$, $EGFRK_{5321884}$, and $EGFRK_{APO}$ complexes are in purple, green, blue, brown and yellow, respectively.

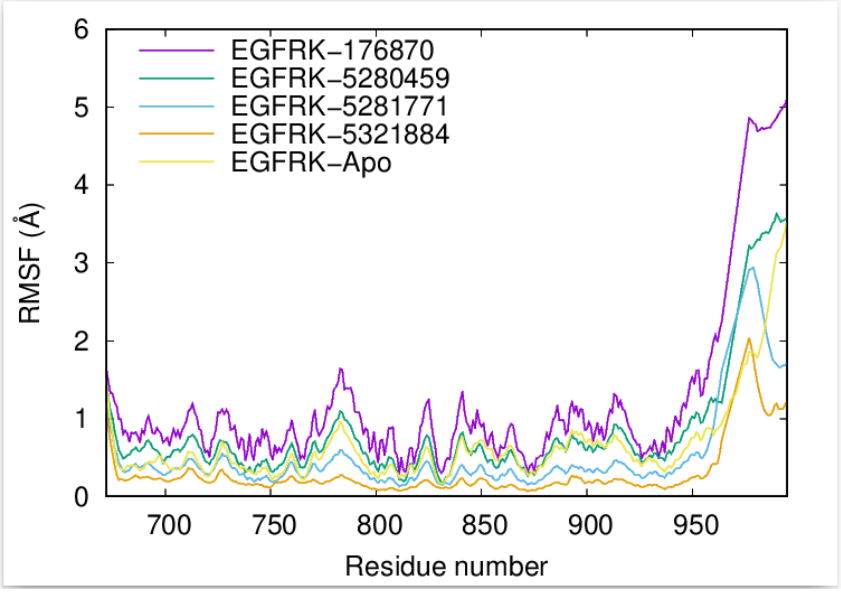

Figure 8. Analysis of RMSF trajectories versus residue number of the four investigated complexes compared with the Protein's Apo structure over 100 ns. Trajectories for $EGFRK_{176870}$, $EGFRK_{5280459}$, $EGFRK_{5281771}$, $EGFRK_{5321884}$, and $EGFRK_{APO}$ complexes are in purple, green, blue, brown and yellow, respectively.

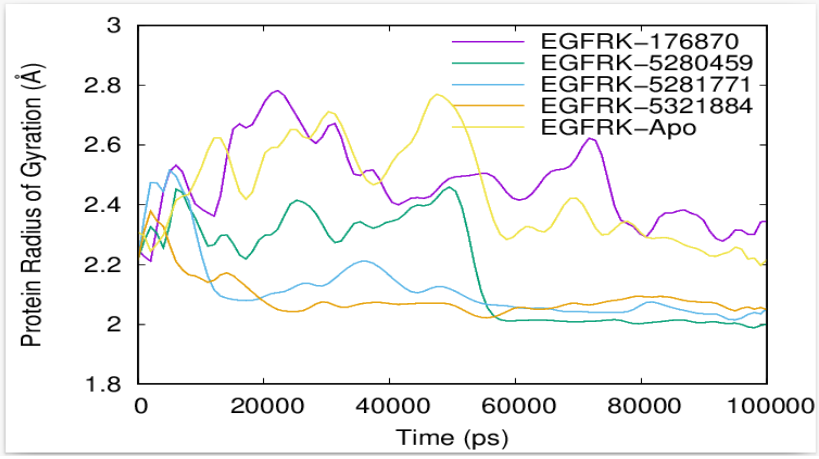

Figure 9. Time-evolution Rg trajectories of the four investigated complexes in comparison with the Protein's Apo structure over 100 ns. Trajectories for $EGFRK_{176870}$, $EGFRK_{5280459}$, $EGFRK_{5281771}$, $EGFRK_{5321884}$, and $EGFRK_{APO}$ complexes are in purple, green, blue, brown and yellow, respectively.

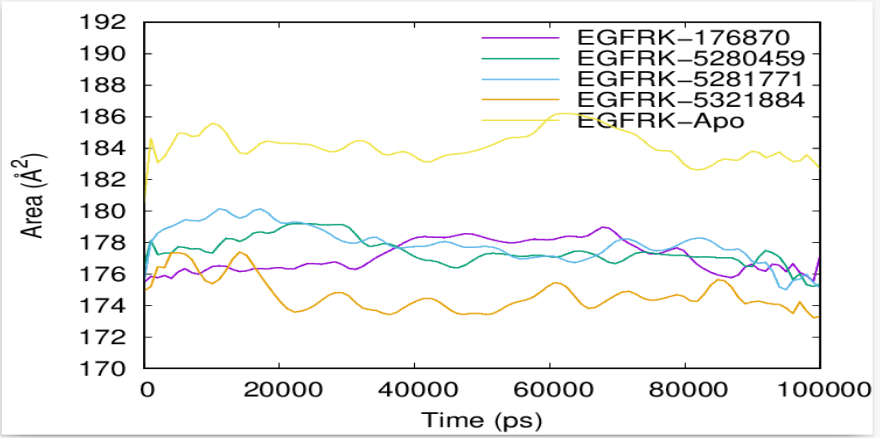

Figure 10. Time-evolution SASA trajectories of the four investigated complexes compared to the Protein's Apo structure over 100 ns. Trajectories for $EGFRK_{176870}$, $EGFRK_{5280459}$, $EGFRK_{5281771}$, $EGFRK_{5321884}$, and $EGFRK_{APO}$ complexes are in purple, green, blue, brown and yellow, respectively.

4. Conclusions

Due to their robust structural complexity, natural products are important sources of hit and lead molecules for discovering novel cancer treatments. This present study used *in silico* tools to investigate a series of phytochemicals from anti-cancer plants and their molecular interactions with the EGFR tyrosine kinase. Three hit compounds, namely, echinacoside, quercitrin, and 2-HPHOT, demonstrated greater binding affinity with the target than erlotinib, a standard anti-cancer drug. Also, echinacoside and 2-HPHOT were stable in MD simulation environments. The findings of this study show that these bioactive molecules could be further explored to discover new compounds that are effective against breast cancer.

Funding

This research received no external funding.

Acknowledgments

My gratitude goes to Adekunle Ajasin University for creating an enabling environment to carry out this research work.

Conflicts of Interest

The authors declare no conflict of interest.

References

1. Cancer. (n.d.). Retrieved August 8, **2021**, from https://www.who.int/news-room/fact-sheets/detail/cancer, 2021.
2. Smolarz, B.; Zadro, A.; Romanowicz, H. Breast Cancer—Epidemiology, Classification, Pathogenesis and Treatment (Review of Literature). *Cancers* **2022,** *14*, https://doi.org/10.3390/cancers14102569.
3. van Seijen, M.; Lips, E.H.; Thompson, A.M.; Nik-Zainal, S.; Futreal, A.; Hwang, E.S.; Verschuur, E.; Lane, J.; Jonkers, J.; Rea, D.W.; Wesseling, J. Ductal carcinoma in situ: to treat or not to treat, that is the question. *British Journal of Cancer* **2019,** *121*, 285–292, https://doi.org/10.1038/s41416-019-0478-6.
4. Grimm, L.J.; Rahbar, H.; Abdelmalak, M.; Hall, A.H.; Ryser, M.D. Ductal Carcinoma in Situ: State-of-the-Art Review. *Radiology* **2022,** *302*, 246-255, https://doi.org/10.1148/radiol.211839.
5. Arnold, M.; Morgan, E.; Rumgay, H.; Mafra, A.; Singh, D.; Laversanne, M.; Vignat, J.; Gralow, J.R.; Cardoso, F.; Siesling, S.; Soerjomataram, I. Current and future burden of breast cancer: Global statistics for 2020 and 2040. *Breast* **2022,** *66*, 15–23, https://doi.org/10.1016/j.breast.2022.08.010.

6. Osei-afriyie, S.; Addae, A.K.; Oppong, S.; Amu, H.; Ampofo, E.; Osei, E. Breast cancer awareness , risk factors and screening practices among future health professionals in Ghana : A cross-sectional study. *PLos One*. **2021,** *16*, https://doi.org/10.1371/journal.pone.0253373.
7. Lukasiewicz, S.; Czeczelewski, M.; Forma, A.; Baj, J.; Sitarz, R.; Stanislawek, A. Breast Cancer—Epidemiology, Risk Factors, Classification, Prognostic Markers, and Current Treatment Strategies—An Updated Review. *Cancers* **2021**, *13*, https://doi.org/10.3390/cancers13174287.
8. Nagata, C.; Mizoue, T.; Tanaka, K.; Tsuji, I.; Wakai.; Inoue, M,; Tsugane, S. Tobacco smoking and breast cancer risk: An evaluation based on a systematic review of epidemiological evidence among the japanese population. *Japanese Journal of Clinical Oncology* **2006,** *36*, 387–394, https://doi.org/10.1093/jjco/hyl031.
9. Ferlay, J.; Seorjomaratam, I.; Dikshit, R.; Eser, S.; Mathers, C.; Rebelo, M.; Parkin, D.M.; Forman, D.; Bray, F. Cancer incidence and mortality worldwide: sources , methods and major patterns in GLOBOCAN 2012. *International Journal of Cancer* **2015**, *136*, E359-86, https://doi.org/10.1002/ijc.29210.
10. Kish, P.; Price, C.J. Life-Threatening Reaction with Topical 5-Fluorouracil. *Drug Safety - Case Reports* **2018,** *5*, 1–3, https://doi.org/10.1007/s40800-017-0068-6.
11. Haidinger, R.; Bauerfeind, I. Long-Term side effects of adjuvant therapy in primary breast cancer patients: Results of a web-based survey. *Breast Care*, **2019,** *14*, 111–116, https://doi.org/10.1159/000497233.
12. Batiha, G. E.; Beshbishy, A. M..; Wasef, L.G.; Elewa, Y.H.A.; Al-Sagan, A.A.; El-Hack, M.E.A.; Taha, A.E.; Abd-Elhakim, Y.M.; Devkota, H.P. Chemical Constituents and Pharmacological Activities of Garlic (Allium sativum L.): A Review. *Nutrients* **2020,** *12*, https://doi.org/10.3390/nu12030872.
13. Shrihastini, V.; Muthuramalingam, P.; Adarshan, S.; Sujitha, M.; Chen, J.; Shin, H.; Ramesh, M. Plant Derived Bioactive Compounds, Their Anti-Cancer Effects and In Silico Approaches as an Alternative Target Treatment Strategy for Breast Cancer: An Updated Overview. *Cancers* **2021,** *13*, https://doi.org/10.3390/cancers13246222.
14. Gutiérrez, A.L.; Barrantes, J.B.; Navarro, M.P.; Monge, M.C.O.; Vargas, M.J.C.; Redondo, G.L.M. General aspects about Allium sativum– a review. *Ars Pharmaceutica (Internet)* **2021,** *62*, 471–481, https://doi.org/10.30827/ars.v62i4.20843.
15. Burlou-Nagy, C.; Banica, F.; Jurca, T.; Vicas, L.G.; Marian, E.; Muresan, M.E.; Bacskay, I.; Kiss, R.; Feher, P.; Pallag, A. Echinacea purpurea (L.) Moench: Biological and Pharmacological Properties— A Review. *Plants* **2022,** *11*, https://doi.org/10.3390/plants11091244.
16. Gurunanselage Don, R.A.S.; Yap, M.K.K. Arctium lappa L. root extract induces cell death via mitochondrial-mediated caspase-dependent apoptosis in Jurkat human leukemic T cells. *Biomedicine and Pharmacotherapy* **2019,** *110*, 918–929, https://doi.org/10.1016/j.biopha.2018.12.023.
17. Mele, M.A. Bioactive compounds and biological activity of ginger. *Journal of Multidisciplinary Sciences*. **2019**, *1*, 1-7, https://doi.org/10.33888/jms.2019.111.
18. Paul, R.; Prasad, M.; Sah, N.K. Anti-cancer biology of *Azadirachta indica* L (neem): A mini review. *Cancer Biology and Therapy*. **2011,** *12*, 467-476, https://doi.org/10.4161/cbt.12.6.16850.
19. Nagini, S.; Nivetha, R.; Palrasu, M.; Mishra, R. Nimbolide, a Neem Limonoid, Is a Promising Candidate for the Anti-cancer Drug Arsenal. *Journal of Medicinal Chemistry* **2021,** *64*, 3560-3577, https://doi.org/10.1021/acs.jmedchem.0c02239.
20. Gabr, S.A.; Alghadir, A.H. Potential anti-cancer activities of Rhus coriaria (sumac) extract against human cancer cell lines. *Bioscience Reports* **2021,** *41*, 1–12, https://doi.org/10.1042/BSR20204384.
21. Kooti, W.; Servatyari, K.; Behzadifar, M.; Asadi-Samani, M.; Sadeghi, F.; Nouri, B.; Marzouni, H.Z. Effective Medicinal Plant in Cancer Treatment, Part 2: Review Study. *Topical Review Article* **2017,** *22*, 982–995, https://doi.org/10.1177/2156587217696927.
22. Sastry, G.M.; Adzhigirey, M.; Day, T.; Annabhimoju, R.; Sherman, W. Protein and ligand preparation: Parameters, protocols, and influence on virtual screening enrichments. *Journal of Computer-Aided Molecular Design* **2013,** *27*, 221–234, https://doi.org/10.1007/s10822-013-9644-8.
23. Friesner, R.A.; Murphy, R.B.; Repasky, M.P.; Frye, L.L.; Greenwood, J.R.; Halgren, T.A.; Sanschagrin, P.C.; Mainz, D.T. Extra precision glide: docking and scoring incorporating a model of hydrophobic enclosure for protein-ligand complexes. *Journal of Medicinal Chemistry* **2006,** *49*, 6177–6196, https://doi.org/10.1021/jm051256o.
24. 24.. Omoboyowa, D.A.; Iqbal, M.N.; Balogun, T.A.; Bodun, D.S.; Fatoki, J.O.; Oyeneyin, O.E. Inhibitory potential of phytochemicals from Chromolaena odorata L. against apoptosis signal-regulatory kinase 1: A computational model against colorectal cancer. *Computational Toxicology* **2022,** *23*, https://doi.org/10.1016/j.comtox.2022.100235.
25. Omoboyowa, D.A.; Singh, G.; Fatoki, J.O.; Oyeneyin, O.E. Computational investigation of phytochemicals from Abrus precatorius seeds as modulators of peroxisome proliferator-activated receptor gamma (PPARγ). *Journal of Biomolecular Structure and Dynamics* **2022,** *40*, 1–15, https://doi.org/10.1080/07391102.2022.2091657.
26. Omoboyowa, D.A. Exploring molecular docking with E-pharmacophore and QSAR models to predict potent inhibitors of 14-α-demethylase protease from Moringa spp. *Pharmacological Research - Modern Chinese Medicine* **2022,** *4*, https://doi.org/10.1016/j.prmcm.2022.100147.

27. Berendsen, H.J.C.; Postma, J.P.M.; Van Gunsteren, W.F.; Dinola, A.; Haak, J.R. Molecular dynamics with coupling to an external bath. *The Journal of Chemical Physics* **1984**, *81*, 3684–3690, https://doi.org/10.1063/1.448118.
28. Parrinello, M.J.; Rahman, A. Polymorphic transitions in single crystals: A new molecular dynamics method. *Journal of Applied Physics* **1981**, *52*, 7182–7190, https://doi.org/10.1063/1.328693.
29. Hess, B.; Bekker, H.; Berendsen, H.J.C.; Fraaije, J.G.E.M. LINCS: A Linear Constraint Solver for molecular simulations. *Journal of Computational Chemistry* **1997,** *18*, 1463–1472, https://doi.org/10.1002/(SICI)1096-987X(199709)18:12<1463::AID-JCC4>3.0.CO;2-H.
30. GROMACS. Welcome to the GROMACS documentation! — GROMACS 2021.5 documentation. **2022**.
31. Lee, J.; Cheng, X.; Swails, J.M.; Yeom, M.S.; Eastman, P.K.; Lemku, J.A.; Wei, S.; Buckner, J.; Jeong, J.C.; Qi, Y.; Jo, S.; Pande, V.S.; Case, D.A.; Brooks, C.L.; Mackerell, A.D.; Klauda, J.B.; Im, W. CHARMM-GUI Input Generator for NAMD, GROMACS, AMBER, OpenMM, and CHARMM/OpenMM Simulations Using the CHARMM36 Additive Force Field. *Journal of Chemical Theory and Computation* **2016,** *12*, 405–413, https://doi.org/10.1021/acs.jctc.5b00935.
32. Olanrewaju, A.A.; Ibeji, C.U.; Oyeneyin, O.E. Biological evaluation and molecular docking of some newly synthesized 3d-series metal(II) mixed-ligand complexes of fluoro-naphthyl diketone and dithiocarbamate. *SN Applied Sciences* **2020,** *2*, https://doi.org/10.1007/s42452-020-2482-0.
33. Genheden, S.; Ryde, U. The MM/PBSA and MM/GBSA methods to estimate ligand-binding affinities. *Expert Opinion on Drug Discovery* **2015,** *10*, 449–461, https://doi.org/10.1517/17460441.2015.1032936.
34. Oyeneyin, O.E.; Obadawo, B.S.; Orimoloye, S.M.; Akintemi, E.O.; Ipinloju, N.; Asere, A.M.; Owolabi, T.O. Prediction of Inhibition Activity of BET Bromodomain Inhibitors using Grid Search-Based Extreme Learning Machine and Molecular Docking. *Letters in Drug Design & Discovery* **2021,** *18*, 1039–1049, https://doi.org/10.2174/1570180818666210521215433.
35. Owolabi, T.O.; Saleh, T.A.; Olusayo, O.; Souiyah, M.; Oyeneyin, O.E. Modeling the Specific Surface Area of Doped Spinel Ferrite Nanomaterials Using Hybrid Intelligent Computational Method. *Journal of Nanomaterials* **2021,** *2021*, https://doi.org/10.1155/2021/9677423.
36. Alqahtani, A.; Saliu, S.; Owolabi, T.O.; Aldhafferi, N.; Almurayh, A.; Oyeneyin, O.E. Modeling the magnetic cooling efficiency of spinel ferrite magnetocaloric compounds for magnetic refrigeration application using hybrid intelligent computational methods. *Materials Today Communications* **2022,** *33*, https://doi.org/10.1016/j.mtcomm.2022.104310.
37. Stamos, J.; Sliwkowski, M.X.; Eigenbrot, C. Structure of the epidermal growth factor receptor kinase domain alone and in complex with a 4-anilinoquinazoline inhibitor. *Journal of Biological Chemistry* **2002,** *277*, 46265–46272, https://doi.org/10.1074/jbc.M207135200.